ChemPubSoc Europe

DOI: 10.1002/chem.201400136

CHEMISTRY A European Journal Communication

Upconversion

Near-Infrared-Light-Driven Artificial Photosynthesis by Nanobiocatalytic Assemblies

Joon Seok Lee, Dong Heon Nam, Su Keun Kuk, and Chan Beum Park*[a]

Abstract: Artificial photosynthesis in nanobiocatalytic assemblies aims to reconstruct man-made photosensitizers, electron mediators, electron donors, and redox enzymes for solar synthesis of valuable chemicals through photochemical cofactor regeneration. Herein, we report, for the first time, on nanobiocatalytic artificial photosynthesis in near-infrared (NIR) light, which constitutes over 46% of the solar energy. For NIR-light-driven photoenzymatic synthesis, we synthesized silica-coated upconversion nanoparticles, Si-NaYF4:Yb,Er and Si-NaYF4:Yb,Tm, for efficient photon-conversion through Förster resonance energy transfer (FRET) with rose bengal (RB), a photosensitizer. We observed NIR-induced electron transfer by using linear sweep voltammetric analysis; this indicates that photoexcited electrons of RB/Si-NaYF4:Yb,Er are transferred to NAD+ through a Rh-based electron mediator. RB/Si-NaYF4:Yb,Er nanoparticles, which exhibit higher FRET efficiency due to more spectral overlap than RB/Si-NaYF4:Yb,Tm, perform much better in the photoenzymatic conversion.

The global increase in power demand and the likely demise of fossil-fuel supplies within the next few decades drive the development of renewable energy resources and other green technologies. Among various options, solar energy has attracted much attention because of the huge amount of energy continuously transferred from the sun to the Earth. Since Fujishima and Honda first discovered photocatalytic water splitting on crystalline TiO_2 electrodes in 1972,[1] many efforts have been devoted to develop photocatalytic devices for efficient solar-energy usage.[2] Numerous photosensitizing systems for light harvesting have been studied over the decades, however, most photosensitizers possess a large bandgap (>1.7 eV) that require ultraviolet (UV) and visible light for activation. Considering that over 46% of the solar energy is in the near-infrared (NIR) range,[3] almost half of the solar spectrum cannot be utilized to activate those photosensitizers. In this respect, rare-earth-doped (e.g., Y, Yb, Er, Tm) upconversion nanoparticles have come into the spotlight as promising material to assist the harvesting of long-wavelength light by transforming NIR light into UV and visible light.[4] Upconversion refers to nonlinear optical processes that occur through anti-Stokes emission, in which an emitted photon has more energy than the absorbed photon by sequential absorption of photons.[5]

In this communication, we report on NIR-light-driven biocatalytic artificial photosynthesis by using upconversion nanoparticles. Artificial photosynthesis is a solar-to-chemical energy-conversion process based on the principle of natural photosynthesis that exhibits remarkable features, such as near-unity quantum yield and environmental compatibility. Biocatalytic artificial photosynthesis is achieved through the integration of photocatalytic and biocatalytic cycles utilizing highly sophisticated catalytic reactions by redox enzymes.[2e] Whereas a sustainable supply of nicotinamide cofactors (e.g., NADH, NADPH), which serve as a reducing equivalent in numerous redox biocatalytic reactions, remains one of the major obstacles in broad applications of redox enzymes,[6] the photon-conversion system can regenerate cofactors in situ through photoinduced electron transfer as in natural photosynthetic processes.[7] In contrast to UV and visible light, NIR light has not yet been utilized for photochemical cofactor regeneration even though it possesses almost half of the solar spectrum. In this regard, upconversion nanoparticles with anti-Stokes emission are promising candidates for an NIR-light harvester to facilitate efficient solar-energy utilization for biocatalytic artificial photosynthesis. Among various upconversion nanoparticles, Yb/Er (or Yb/Tm) co-doped $NaYF_4$ nanoparticles exhibit the highest NIR-to-visible upconversion efficiency, because the Yb^{3+} ion is an efficient NIR antenna with a long-lifetime-excited energy level.[4,8] Herein, we utilized $NaYF_4$:Yb,Er nanoparticles for upconversion and rose bengal (RB) for enhancing photon-conversion efficiency through FRET (Förster resonance energy transfer). RB is known to possess a good photochemical redox property, because of the internal singlet–triplet transition by light absorption,[9] and has adequate optical properties for FRET with the $NaYF_4$:Yb,Er nanoparticles.

Our approach to NIR-light-driven photoenzymatic synthesis with FRET-conjugated upconversion nanoparticles is shown in Figure 1. Under the irradiation of NIR light, the absorption of pump photons populates the $^4F_{7/2}$ level of the Er^{3+} ions through energy transfer from excited Yb^{3+} ions. The $^4F_{7/2}$ level can decay nonradiatively to the $^2H_{11/2}$, $^4S_{3/2}$, and $^4F_{9/2}$ levels, then multiphonon nonradiative relaxation from these levels to the $^4I_{15/2}$ level induces green emission bands around 520 and 540 nm, and red emission band at 660 nm.[4,10] The absorption

[a] Dr. J. S. Lee,[+] D. H. Nam,[+] S. K. Kuk, Prof. Dr. C. B. Park
Department of Materials Science and Engineering
Korea Advanced Institute of Science and Technology (KAIST)
335 Science Road, Daejeon 305-701 (Republic of Korea)
E-mail: parkcb@kaist.ac.kr

[+] These authors contributed equally to this work.

Supporting information for this article is available on the WWW under http://dx.doi.org/10.1002/chem.201400136.

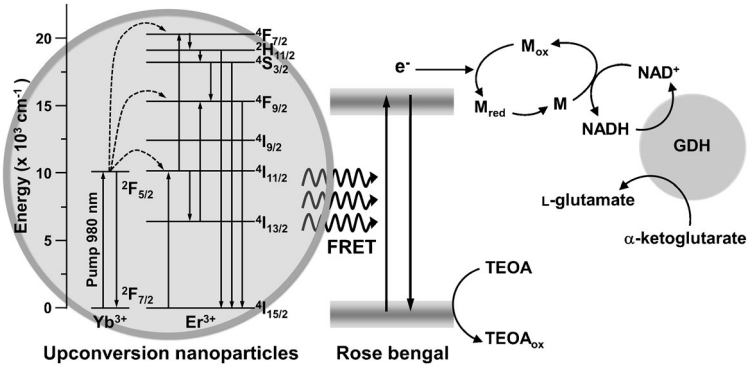

Figure 1. Schematic diagram of NIR-light-driven biocatalytic artificial photosynthesis with FRET-conjugated upconversion nanoparticles. The photoexcited electrons generated by RB/Si-$NaYF_4$:Yb,Er are transferred to NAD^+ through the rhodium(III)-based mediator (**M**), and then used to synthesize L-glutamate by GDH. TEOA = triethanolamine.

band of RB (450–600 nm) overlaps well with the green emission band of $NaYF_4$:Yb,Er nanoparticles (see the Supporting Information, Figure S1). In addition, electrostatic interaction of $NaYF_4$:Yb,Er nanoparticles and RB ensures the close proximity (Figure 3, to be discussed later). Taken together, energy transfer from upconversion nanoparticles to RB occurs upon 980 nm excitation through FRET. According to the literature,[11] RB exhibits a red emission band with a microsecond-scale lifetime through singlet-to-triplet intersystem crossing. The fluorescence lifetime of RB is approximately 0.1 ps.[12] Because many RB molecules can bind to a single $NaYF_4$:Yb,Er nanoparticle, photon-conversion of FRET-conjugated upconversion nanoparticles is more efficient than for bare nanoparticles. NIR-excited electrons by FRET are then transferred to a rhodium-(III)-based mediator (**M** = $[Cp^*Rh(bpy)H_2O]^+$, $Cp^* = C_5Me_5$, bpy = 2,2′-bipyridine), and used to reduce NAD^+ to NADH for the synthesis of L-glutamate by NADH-dependent L-glutamate dehydrogenase (GDH). The organometallic compound, **M**, is used as a primary mediator to transfer hydrides in the cofactor-regeneration system. According to the literature,[13] $\mathbf{M_{ox}}$ is reduced to $\mathbf{M_{red}}$ by accepting two photoexcited electrons from the FRET-conjugated upconversion nanoparticles, then $\mathbf{M_{red}}$ is chemically converted to the **M** by taking up one proton from an aqueous solution. NADH is produced from NAD^+ by accepting hydride from **M** that is then oxidized to $\mathbf{M_{ox}}$. Due to its high regioselectivity (> 99%) over broad pH and temperature ranges, **M** enables the regeneration of enzymatically active cofactors.[13a,14]

Our synthesized $NaYF_4$:Yb,Er nanoparticles had a polyhedral shape, good uniformity, and monodispersity with an average diameter of approximately 55 nm (Figure 2a,b). According to the high-resolution TEM image (Figure 2c), a crystal lattice of the (100) plane with an interplanar spacing of 0.52 nm was observed; this indicates high crystallinity of the $NaYF_4$:Yb,Er nanoparticles. Selected-area electron diffraction (SAED) and XRD patterns (Figure 2d,e) further confirmed the crystal structure of the $NaYF_4$:Yb,Er nanoparticles. All of the diffraction peaks matched the JCPDS PDF peak (#28-1192) well, suggesting a hexagonal phase with cell parameters of $a = 5.96$ Å and $c = 3.51$ Å. No impurity peak was observed, indicating high purity of the final material.

To prepare FRET-conjugated $NaYF_4$:Yb,Er nanoparticles, we coated a thin and uniform silica shell on each nanoparticle through the modified water-in-oil microemulsion method.[15] The thickness of the silica shell was approximately 8 nm and the silica-coated $NaYF_4$:Yb,Er nanoparticles (Si-$NaYF_4$:Yb,Er) were well-dispersed in aqueous solutions (Figure 3a). After silica coating, Si-$NaYF_4$:Yb,Er was treated with 3-aminopropyltrimethoxysilane to have a positively charged amine functional group on the surface for binding RB through electrostatic interactions. Figure 3b shows that the zeta potentials of bare and NH_2-treated Si-$NaYF_4$:Yb,Er were −23.3 and 53.6 mV, respectively, confirming successful functionalization of the Si-$NaYF_4$:Yb,Er surface by positively charged groups. The zeta potential of the NH_2-treated Si-$NaYF_4$:Yb,Er drastically decreased from 53.6 to 15.2 mV upon binding of RB molecules on the $NaYF_4$:Yb,Er nanoparticles. We also observed that RB/silica-coated $NaYF_4$:Yb,Er nanoparticles (RB/Si-$NaYF_4$:Yb,Er) had an absorption peak at 550 nm and exhibited a red emission band under 980 nm excitation (Figure 3c,d). In contrast to RB/Si-$NaYF_4$:Yb,Er, Si-$NaYF_4$:Yb,Er showed no absorption peak at 550 nm and exhibited a green emission band. These results support that the RB molecules were successfully bound to the $NaYF_4$:Yb,Er nanoparticles. To confirm the proximity between the $NaYF_4$:Yb,Er nanoparticles and the RB molecules, we analyzed RB/Si-$NaYF_4$:Yb,Er by using TEM (see the Supporting Information, Figure S2a). The thickness of the silica shell did not change compared with that of

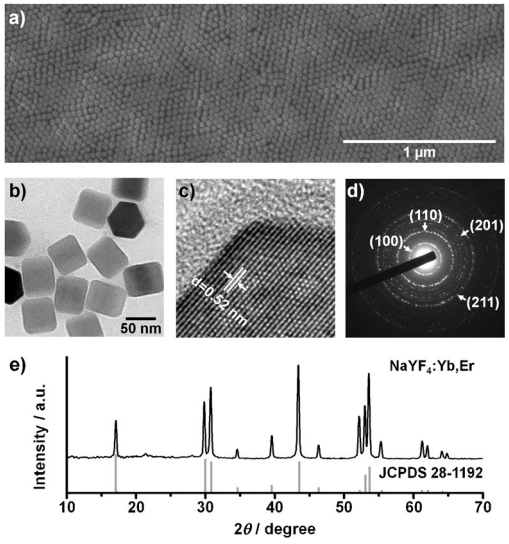

Figure 2. Morphology analysis of $NaYF_4$:Yb,Er nanoparticles by a) SEM and b) TEM. The $NaYF_4$:Yb,Er nanoparticles exhibit polyhedral shape, good uniformity, and monodispersity with an average diameter of approximately 55 nm. c) The HRTEM images of a $NaYF_4$:Yb,Er nanoparticle show a crystal lattice of the (100) plane with an interplanar spacing of 0.52 nm. d) SAED and e) XRD patterns of $NaYF_4$:Yb,Er nanoparticles indicate that the crystal structure of the nanoparticles is in the hexagonal phase with cell parameters of $a = 5.96$ Å and $c = 3.51$ Å.

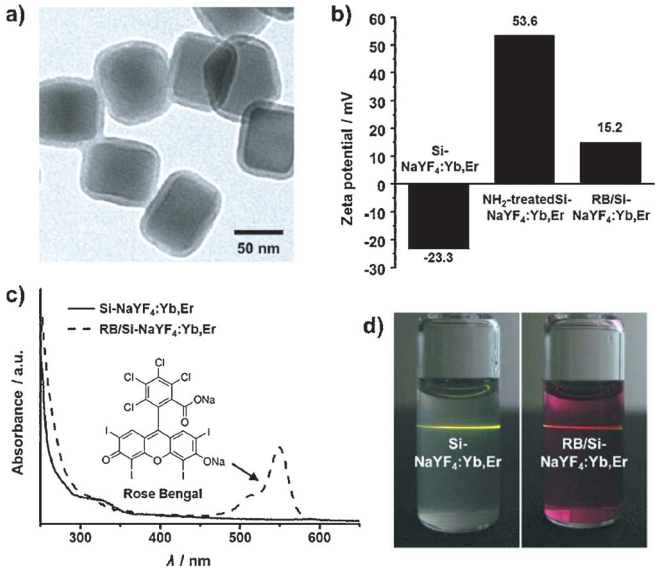

Figure 3. a) TEM images of silica-coated $NaYF_4$:Yb,Er nanoparticles (Si-$NaYF_4$:Yb,Er) dispersed in aqueous solutions. b) Zeta potentials of bare, NH_2-treated, and RB-bound Si-$NaYF_4$:Yb,Er, showing successful binding of RB molecules on the $NaYF_4$:Yb,Er nanoparticles. c) Absorption spectra of Si-$NaYF_4$:Yb,Er with and without RB. d) Digital camera images of upconversion nanoparticles upon the irradiation of a 980 nm laser.

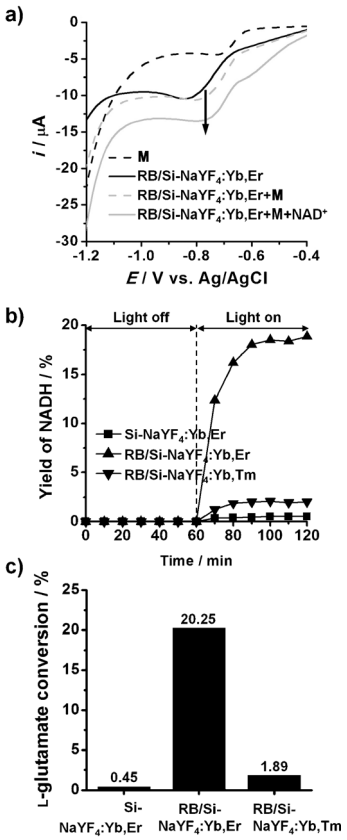

Figure 4. a) Linear sweep voltammograms of RB/Si-$NaYF_4$:Yb,Er in the absence and presence of **M** and NAD^+. RB/Si-$NaYF_4$:Yb,Er with **M** exhibits a strong increment in the reduction-peak current with the addition NAD^+, indicating the catalytic effect on the reduction reaction of NAD^+. NIR-light-driven b) photochemical NADH regeneration and c) photoenzymatic synthesis of L-glutamate with upconversion nanoparticles. RB/Si-$NaYF_4$:Yb,Er exhibits the highest performance; this indicates that the FRET between RB and the upconversion nanoparticles is critical for photon-conversion efficiency and NIR-light-driven biocatalytic artificial photosynthesis.

Si-$NaYF_4$:Yb,Er; this indicates electrostatic interactions between the $NaYF_4$:Yb,Er nanoparticles and the RB molecules and ensures a close proximity between them for the FRET process.

We conducted linear sweep voltammetry to investigate whether photoexcited electrons generated by RB/Si-$NaYF_4$:Yb,Er were transferred to NAD^+ via **M**. As shown in Figure 4a, the reduction-peak potential of **M** and RB/Si-$NaYF_4$:Yb,Er appeared at −0.70 and −0.84 V, respectively. **M** exhibited a broad reduction peak; this means that the disproportionation reaction of **M** to $\mathbf{M_{ox}}$ and $\mathbf{M_{red}}$ occurs under our experimental conditions according to the literature.[16] When RB/Si-$NaYF_4$:Yb,Er and **M** were present in solution at the same time, the reduction-peak current was observed at −0.75 V, indicating co-reduction of these two components. Upon the addition of NAD^+, the reduction-peak current of RB/Si-$NaYF_4$:Yb,Er with **M** increased significantly, implying a catalytic effect on the reduction reaction of NAD^+. Our results show that NIR-excited electrons of RB/Si-$NaYF_4$:Yb,Er were transferred to NAD^+ through **M** to photochemically regenerate NADH by FRET-conjugated $NaYF_4$:Yb,Er nanoparticles. We compared the FRET efficiency on NADH regeneration by using different upconversion materials: RB/Si-$NaYF_4$:Yb,Er versus RB/Si-$NaYF_4$:Yb,Tm (Figure 4b). RB/Si-$NaYF_4$:Yb,Tm nanoparticles were prepared by the same method used for the synthesis of RB/Si-$NaYF_4$:Yb,Er (see the Supporting Information, Figure S2b, c).[15a,17] According to our result, the irradiation of NIR light induced an immediate reduction of NAD^+ to NADH in the presence of upconversion nanoparticles, whereas NAD^+ was not reduced at all in the absence of light. In particular, the yield of NADH conversion during 1 h was 9 and 35 times higher with RB/Si-$NaYF_4$:Yb,Er (18.86%) than with RB/Si-$NaYF_4$:Yb,Tm and Si-$NaYF_4$:Yb,Er, respectively. We attribute these results to the different FRET efficiencies between upconversion nanoparticles. In the case of RB/Si-$NaYF_4$:Yb,Tm, the emission band of $NaYF_4$:Yb,Tm nanoparticles overlaps only slightly with the absorption band of RB, because Tm^{3+} emits in the blue (450 and 480 nm) and red (660 nm) regions by multiphonon nonradiative relaxations: 450 nm for $^1D_2$ to $^3F_4$, 480 nm for $^1G_4$ to $^3H_6$, 660 nm for $^1G_4$ to $^3F_4$ (see the Supporting Information, Figure S3).[3–4] Thus, the FRET efficiency of RB/Si-$NaYF_4$:Yb,Tm should be much lower than that of RB/Si-$NaYF_4$:Yb,Er, because the energy-transfer rate is directly related to the spectral overlap. The FRET efficiency of Si-$NaYF_4$:Yb,Er is null due to the absence of an FRET acceptor (i.e., RB). These results indicate that FRET between RB and upconversion nanoparticles is critical for photon-conversion efficiency and NIR-light-driven photochemical NADH reduction. Considering that biocatalytic artificial photosynthesis is achieved by integral coupling of photocatalysis and biocatalysis cycles, we performed photochemical NADH regeneration and photoenzymatic synthesis under the irradiation of 980 nm light by using GDH as a model NADH-dependent enzyme (Figure 4c). The conversion yield of L-glutamate with RB/Si-$NaYF_4$:Yb,Er was 20.25% after 5 h, whereas those with Si-NaY-

F_4:Yb,Er and RB/Si-$NaYF_4$:Yb,Tm were 0.45% and 1.89%, respectively; this demonstrates that redox enzymatic conversion of α-ketoglutarate to L-glutamate is highly facilitated with RB/Si-$NaYF_4$:Yb,Er through NIR-light-driven photochemical NADH regeneration. Taken together, our results indicate that upconversion nanoparticles with anti-Stokes emission are promising light harvesters for efficient utilization of the NIR region of solar energy during biocatalytic artificial photosynthesis.

In summary, we have demonstrated for the first time photoenzymatic synthesis of chemicals with upconversion nanoparticles through NIR-light-driven cofactor regeneration. From the zeta potential and spectrofluorometric analyses, we verified successful binding of RB molecules to $NaYF_4$:Yb,Er nanoparticles through electrostatic interactions over distances that are short enough for FRET to occur. NIR-induced electron transfer was observed through linear sweep voltammetric analysis, which indicated that photoexcited electrons of RB/Si-$NaYF_4$:Yb,Er were transferred to NAD^+ through **M**, an electron mediator. By comparing RB/Si-$NaYF_4$:Yb,Er with RB/Si-$NaYF_4$:Yb,Tm and Si-$NaYF_4$:Yb,Er, we investigated the effect of FRET efficiency on redox enzymatic reaction coupled with NIR-light-driven NADH regeneration. RB/Si-$NaYF_4$:Yb,Er nanoparticles, which exhibit higher FRET efficiency due to more spectral overlap than RB/Si-$NaYF_4$:Yb,Tm, resulted in better performance for the photoenzymatic conversion of α-ketoglutarate to L-glutamate. Our research shows that upconversion nanoparticles with anti-Stokes emission are promising light harvesters for versatile usage of NIR light in solar-to-chemical conversion processes.

Experimental Section

Materials

All chemicals were purchased from Sigma–Aldrich (St. Louis, MO) in reagent grade purity and were used without further purification. The rhodium(III)-based electron mediator (**M** = $[Cp^*Rh(bpy)H_2O]^+$, $Cp^* = C_5Me_5$, bpy = 2,2′-bipyridine) was synthesized according to the method reported previously.[13a]

Synthesis of upconversion nanoparticles

$NaYF_4$:Yb(18%),Er(2%) nanoparticles were synthesized according to the method reported previously.[8,15,17] YCl_3 (0.8 mmol), $YbCl_3$ (0.18 mmol), $ErCl_3$ (0.02 mmol), and oleic acid (6 mL) were added in 1-octadecene (15 mL). The homogeneous solution was formed by heating to 160 °C, and then cooling to 50 °C. A methanol solution (10 mL) containing NaOH (2.5 mmol) and NH_4F (4 mmol) was slowly added into the homogeneous solution and stirred for 30 min. To remove methanol, the solution was kept at 100 °C for 10 min, then maintained at 310 °C for 1 h under argon atmosphere. After the solution had cooled naturally, nanoparticles precipitated with addition of ethanol. The nanoparticles washed with ethanol/water (1:1 v/v) three times. In the synthesis of $NaYF_4$:Yb(20%),Tm-(0.5%) nanoparticles, the above procedure was followed exactly, except for the use of YCl_3 (0.795 mmol), $YbCl_3$ (0.2 mmol), and $TmCl_3$ (0.005 mmol).

Preparation of rose bengal/silica-coated upconversion nanoparticles

To produce silica-coated upconversion nanoparticles, a modified water-in-oil microemulsion method was used.[15] Upconversion nanoparticles, Igepal CO-520, ammonia (wt 28%), and cyclohexane were mixed by ultrasonication until a transparent emulsion was formed. Then, TEOS (tetraethyl orthosilicate) was added into the solution, which was stirred for 36 h. After that, silica-coated upconversion nanoparticles precipitated by the addition of acetone; these were washed with ethanol at least three times, and redispersed in ethanol. For the synthesis of rose bengal/silica-coated upconversion nanoparticles, 3-aminopropyltrimethoxysilane (APTMS) was added to the silica-coated upconversion nanoparticle solution, which was then refluxed for 4 h. The APTMS-treated upconversion nanoparticles were sufficiently rinsed with ethanol to wash away any remaining APTMS moiety. After that, the APTMS-treated upconversion nanoparticles were immersed in a rose bengal solution (100 μM) for 2 h under vigorous stirring. The rose bengal/silica-coated upconversion nanoparticles were isolated by centrifugation and redispersed in water.

Characterization

The morphology of the upconversion nanoparticles was observed with an S-4800 field emission scanning electron microscope (Hitachi High-Technologies, Japan) and a 200 keV field emission transmission electron microscope (JEOL, Model JEM-2100F, Japan). XRD patterns were analyzed with a powder X-ray diffractometer (Rigaku, Model D/MAX-IIIC, Japan) and under the following conditions: $Cu_{K\alpha}$ radiation, $\lambda = 1.5418$ Å; scan speed, $3^\circ min^{-1}$; scan range, 10–70°. UV/Vis absorption spectra were measured with a V-650 spectrophotometer (JASCO, Japan). The zeta potential and spectrofluorometric analysis was performed with a particle size analyzer (Zetasizer Nano ZS, Malvern Instruments, UK) and a spectrofluorophotometer (RF-5301PC, Shimadzu, Japan), respectively. For the electrochemical analysis, upconversion nanoparticles (5 mM), **M** (250 μM), and NAD^+ (1 mM) were dispersed in a phosphate buffer (100 mM, pH 7.0). A three-electrode system was used in order to obtain cyclic voltammograms; a glassy carbon disk (working, 3 mm diameter), Ag/AgCl (reference, 0.197 V vs. normal hydrogen electrode), and a platinum wire (counter) were connected to a multichannels potentiostat/galvanostat (WonATech, Model WMPG1000, Korea) at a scan rate of 100 $mV s^{-1}$.

Photochemical cofactor regeneration and redox enzymatic synthesis

Photochemical regeneration of NADH was performed in a quartz reactor under an Ar atmosphere at room temperature. NAD^+ (1 mM) and **M** (250 μM) were dissolved in a phosphate buffer (100 mM, pH 7.0) containing triethanolamine (15% w/v). Upconversion nanoparticles (5 mM) were dissolved in the reaction solution, which was then exposed to light from a 980 nm diode IR laser system (Dragonlasers, China). The concentration of NADH was measured by analyzing the absorbance at 340 nm with a spectrophotometer (V-650, JASCO, Japan). Photoenzymatic synthesis of L-glutamate was performed in a reaction medium composed of upconversion nanoparticles (5 mM), NAD^+ (0.2 mM), **M** (500 μM), α-ketoglutarate (10 mM), ammonium sulfate (100 mM), and L-glutamate dehydrogenase (40 U) dissolved in a phosphate buffer (100 mM, pH 7.0) containing triethanolamine (15% w/v). High-performance liquid chromatography (LC-20A prominence, Shimadzu, Japan), equipped with an Inertsil C18 column (ODS-3 V, length,

150 mm), was used for the analysis of L-glutamate. Samples were eluted by phosphoric acid (0.085%) at a flow rate of 1.0 mL min^{-1} and detected at 210 nm.

Acknowledgements

This study was supported by grants from the National Research Foundation (NRF) via the National Leading Research Laboratory (NRF-2013R1A2A1A05005468), the Intelligent Synthetic Biology Center of Global Frontier R&D Project (2011–0031957), and the Converging Research Center (2010–50207), Republic of Korea.

Keywords: artificial photosynthesis · cofactor regeneration · FRET · near-infrared light · upconversion

[1] A. Fujishima, K. Honda, *Nature* **1972**, *238*, 37–38.
[2] a) G. K. Mor, O. K. Varghese, R. H. T. Wilke, S. Sharma, K. Shankar, T. J. Latempa, K.-S. Choi, C. A. Grimes, *Nano Lett.* **2008**, *8*, 1906–1911; b) J. C. Ruiz-Morales, D. Marrero-Lopez, M. Galvez-Sanchez, J. Canales-Vazquez, C. Savaniu, S. N. Savvin, *Energy Environ. Sci.* **2010**, *3*, 1670–1681; c) S. Y. Reece, J. A. Hamel, K. Sung, T. D. Jarvi, A. J. Esswein, J. J. H. Pijpers, D. G. Nocera, *Science* **2011**, *334*, 645–648; d) D. G. Nocera, *Acc. Chem. Res.* **2012**, *45*, 767–776; e) S. H. Lee, J. H. Kim, C. B. Park, *Chem. Eur. J.* **2013**, *19*, 4392–4406.
[3] Y. Tang, W. Di, X. Zhai, R. Yang, W. Qin, *ACS Catal.* **2013**, *3*, 405–412.
[4] J. Méndez-Ramos, J. C. Ruiz-Morales, P. Acosta-Mora, J. del-Castillo, A. C. Yanes, *J. Power Sources* **2013**, *238*, 313–317.
[5] M. Haase, H. Schäfer, *Angew. Chem.* **2011**, *123*, 5928–5950; *Angew. Chem. Int. Ed.* **2011**, *50*, 5808–5829.
[6] W. Liu, P. Wang, *Biotechnol. Adv.* **2007**, *25*, 369–384.
[7] a) S. H. Lee, D. H. Nam, J. H. Kim, J.-O. Baeg, C. B. Park, *ChemBioChem* **2009**, *10*, 1621–1624; b) D. H. Nam, S. H. Lee, C. B. Park, *Small* **2010**, *6*, 922–926; c) J. Ryu, S. H. Lee, D. H. Nam, C. B. Park, *Adv. Mater.* **2011**, *23*, 1883–1888; d) J. H. Kim, M. Lee, J. S. Lee, C. B. Park, *Angew. Chem.* **2012**, *124*, 532–535; *Angew. Chem. Int. Ed.* **2012**, *51*, 517–520; e) D. H. Nam, C. B. Park, *Chembiochem* **2012**, *13*, 1278–1282.
[8] H. S. Qian, H. C. Guo, P. C.-L. Ho, R. Mahendran, Y. Zhang, *Small* **2009**, *5*, 2285–2290.
[9] S. H. Lee, D. H. Nam, C. B. Park, *Adv. Synth. Catal.* **2009**, *351*, 2589–2594.
[10] a) J. de Wild, A. Meijerink, J. K. Rath, W. G. J. H. M. van Sark, R. E. I. Schropp, *Energy Environ. Sci.* **2011**, *4*, 4835–4848; b) G. Tian, Z. Gu, L. Zhou, W. Yin, X. Liu, L. Yan, S. Jin, W. Ren, G. Xing, S. Li, Y. Zhao, *Adv. Mater.* **2012**, *24*, 1226–1231.
[11] Y. Wang, K. Liu, X. Liu, K. i. Dohnalová, T. Gregorkiewicz, X. Kong, M. C. G. Aalders, W. J. Buma, H. Zhang, *J. Phys. Chem. Lett.* **2011**, *2*, 2083–2088.
[12] M. A. J. Rodgers, *Chem. Phys. Lett.* **1981**, *78*, 509–514.
[13] a) F. Hollmann, B. Witholt, A. Schmid, *J. Mol. Catal. B* **2002**, *19–20*, 167–176; b) M. M. Grau, M. Poizat, I. W. C. E. Arends, F. Hollmann, *Appl. Organomet. Chem.* **2010**, *24*, 380–385.
[14] H. C. Lo, C. Leiva, O. Buriez, J. B. Kerr, M. M. Olmstead, R. H. Fish, *Inorg. Chem.* **2001**, *40*, 6705–6716.
[15] a) Z. Li, Y. Zhang, S. Jiang, *Adv.Mater.* **2008**, *20*, 4765–4769; b) J. Zhao, Z. Lu, Y. Yin, C. McRae, J. A. Piper, J. M. Dawes, D. Jin, E. M. Goldys, *Nanoscale* **2013**, *5*, 944–952.
[16] a) E. Steckhan, S. Herrmann, R. Ruppert, E. Dietz, M. Frede, E. Spika, *Organometallics* **1991**, *10*, 1568–1577; b) F. Hildebrand, C. Kohlmann, A. Franz, S. Lütz, *Adv. Synth. Catal.* **2008**, *350*, 909–918.
[17] Z. Li, Y. Zhang, *Nanotechnology* **2008**, *19*, 345606.

Received: January 13, 2014
Published online on March 11, 2014